

# Neutrino-driven supernovae: Boltzmann neutrino transport and the explosion mechanism

O. E. B. Messer<sup>†‡</sup> A. Mezzacappa<sup>†‡</sup> S. W. Bruenn<sup>§</sup>, and  
M. W. Guidry<sup>†‡</sup>

† Physics Division, Oak Ridge National Laboratory, Oak Ridge, TN 37831

‡ Department of Physics and Astronomy, University of Tennessee, Knoxville, TN 37996

§ Department of Physics, Florida Atlantic University, Boca Raton, FL 33431

**Abstract.** Core-collapse supernovae are, despite their spectacular visual display, neutrino events. Virtually all ( $\sim 99\%$ ) of the  $10^{53}$  ergs of gravitational binding energy released in the formation of the nascent neutron star is carried away in the form of neutrinos and antineutrinos of all three flavors, and these neutrinos are primarily responsible for powering the explosion. This mechanism depends sensitively on the neutrino transport between the neutrinospheres and the shock. In light of this, we have performed a comparison of multigroup Boltzmann neutrino transport (MGBT) and (Bruenn's) multigroup flux-limited diffusion (MGFLD) in post-core bounce environments. Our analysis concentrates on those quantities central to the postshock matter heating stemming from electron neutrino and antineutrino absorption, namely the neutrino luminosities, RMS energies, and mean inverse flux factors. We show that MGBT yields mean inverse flux factors in the gain region that are  $\sim 25\%$  larger and luminosities that are  $\sim 10\%$  larger than those computed by MGFLD. Differences in the mean inverse flux factors, luminosities, and RMS energies translate to heating rates that are up to 2 times larger for Boltzmann transport, with net cooling rates below the gain radius that are typically  $\sim 0.8$  times the MGFLD rates. These differences are greatest at earlier postbounce times for a given progenitor mass, and for a given postbounce time, greater for greater progenitor mass. The increased differences with increased progenitor mass suggest that the net heating enhancement from MGBT is potentially robust and self-regulated.

## 1. Introduction

Ascertaining the core collapse supernova mechanism is a long-standing problem in astrophysics. The current paradigm begins with the collapse of a massive star's iron core and the generation of an outwardly propagating shock wave that results from core rebound. Because of nuclear dissociation and neutrino losses, the shock stagnates. This sets the

stage for a shock reheating mechanism whereby neutrino energy deposition via electron neutrino and antineutrino absorption on nucleons behind the shock reenergizes it (Bethe & Wilson 1985; Wilson 1985).

The shock reheating phase is essential to the supernova's success, but it is precisely this phase that is difficult to simulate realistically. During shock reheating, core electron neutrinos and antineutrinos are radiated from their respective neutrinospheres, and a small fraction of this radiated energy is absorbed in the exterior shocked mantle. The shock reheating depends sensitively on the electron neutrino and antineutrino luminosities, spectra (best characterized by the RMS energies), and angular distributions in the region behind the shock (e.g., see Burrows & Goshy 1993, Janka & Müller 1996, Mezzacappa *et al* 1998).

These, in turn, depend on the neutrino transport in the semitransparent region encompassing the neutrinospheres, necessitating a neutrino transport treatment that is able to transit accurately and seamlessly between neutrino-thick and neutrino-thin regions.

Various neutrino transport approximations have been implemented in simulating core collapse supernovae. The most sophisticated approximation, which naturally has been used in realistic one-dimensional simulations, is multigroup flux-limited diffusion (MGFLD; e.g., Bowers & Wilson 1982, Bruenn 1985, Myra *et al* 1987). MGFLD closes the neutrino radiation hydrodynamics hierarchy of equations at the level of the first moment (the neutrino flux) by imposing a relationship between the flux and the gradient of the neutrino energy density (the zeroth moment). For example,

$$F_\nu = -\frac{c\Lambda}{3} \frac{\partial U_\nu}{\partial r} + \dots, \quad (1)$$

$$\Lambda = \frac{1}{1/\lambda + |\partial U_\nu / \partial r| / 3U_\nu}, \quad (2)$$

where  $\lambda$  is the neutrino mean free path, and  $U_\nu$  and  $F_\nu$  are the neutrino energy density and flux (Bruenn 1985). [Other forms for the flux-limiter  $\Lambda$  can be found in Bowers & Wilson (1982), Levermore & Pomraning (1981), and Myra *et al* (1987).] Whereas the limits  $\lambda \rightarrow 0$  and  $\lambda \rightarrow \infty$  produce the correct diffusion and free streaming fluxes, it is in the critical intermediate regime where the MGFLD approximation is of unknown accuracy. Unfortunately, the quantities central to the postshock neutrino heating, i.e., the neutrino RMS energies, luminosities, and mean inverse flux factors, are determined in this regime, and given the sensitivity of the neutrino heating to these quantities, it becomes necessary to consider more accurate transport schemes. Moreover, in detailed one-dimensional simulations that have implemented elaborate MGFLD neutrino transport (e.g., see Bruenn 1993, Wilson & Mayle 1993, and Swesty & Lattimer 1994), explosions were not obtained unless the neutrino heating was boosted by additional phenomena, such as convection. This leaves us with at least two possibilities to consider: (1) Failures to produce explosions in the absence of additional phenomena, such as convection, have resulted from neutrino transport approximation. (2) Additional phenomena may be essential in obtaining explosions.

## 2. Initial Models, Codes, and Methodology

We begin with  $15 M_{\odot}$  and  $25 M_{\odot}$  precollapse models S15s7b and S25s7b provided by Woosley (1995). The initial models were evolved through core collapse and bounce using one-dimensional Lagrangian hydrodynamics and MGFLD neutrino transport coupled to the Lattimer-Swesty equation of state (Lattimer & Swesty 1991). The data at 106 ms and 233 ms after bounce for S15s7b and 156 ms after bounce for S25s7b were thermally and hydrodynamically frozen. Stationary-state neutrino distributions were computed for these profiles using both MGBT and MGFLD.

The MGBT simulations were performed using BOLTZTRAN: a Newtonian gravity,  $O(v/c)$ , three-flavor, Boltzmann neutrino transport code developed for the supernova problem and used thus far for studies of stellar core collapse (Mezzacappa and Matzner 1989, Mezzacappa & Bruenn 1993abc). The MGFLD simulations were performed using MGFLD-TRANS: a Newtonian gravity,  $O(v/c)$ , three-flavor, MGFLD neutrino transport code, which has been used for both core collapse and postbounce evolution (e.g., Bruenn 1985, 1993).

The MGBT simulations used 110 nonuniform radial spatial zones and 12 neutrino energy zones spanning a range between 5 and 225 MeV. The MGFLD used the same spatial and energy grids. Simulations with 20 energy zones spanning the same energy range were performed with BOLTZTRAN; no changes in the results presented here were seen.

For the MGBT simulations there is an added dimension: neutrino direction cosine. Because MGBT computes the neutrino distributions as a function of direction cosine and energy for each spatial zone, the isotropy of the neutrino radiation field as a function of radius and neutrino energy is computed from first principles. This is one of the key features distinguishing MGBT and MGFLD. Because the isotropy of the neutrino radiation field is critical to the shock reheating/revival, four Gaussian quadrature sets (2-, 4-, 6-, and 8-point) were implemented in the MGBT simulations to ensure numerical convergence of the results.

## 3. Results

For electron neutrino and antineutrino absorption on neutrons and protons, the neutrino heating rate (in MeV/nucleon) in the region between the neutrinospheres and the shock can be written as

$$\dot{\epsilon} = \frac{X_n}{\lambda_0^a} \frac{L_{\nu_e}}{4\pi r^2} \langle E_{\nu_e}^2 \rangle \langle \frac{1}{F} \rangle + \frac{X_p}{\lambda_0^a} \frac{L_{\bar{\nu}_e}}{4\pi r^2} \langle E_{\bar{\nu}_e}^2 \rangle \langle \frac{1}{\bar{F}} \rangle \quad (3)$$

where:  $\lambda_0^a = \bar{\lambda}_0^a = G_F^2 \rho (g_V^2 + 3g_A^2) / \pi (hc)^4 m_B$ ;  $G_F / (\hbar c)^3 = 1.166 \times 10^{-5} \text{ GeV}^{-2}$  is the Fermi coupling constant;  $\rho$  is the matter density;  $g_V = 1.0$ ,  $g_A = 1.23$ ;  $m_B$  is the baryon mass;  $X_{n,p}$  are the free neutron and proton mass fractions; and  $L_{\nu_e, \bar{\nu}_e}$ ,  $\langle E_{\nu_e, \bar{\nu}_e}^2 \rangle$ , and  $F, \bar{F}$  are the electron neutrino and antineutrino luminosities, RMS energies, and mean inverse flux factors, defined by

$$L_{\nu_e} = 4\pi r^2 \frac{2\pi c}{(hc)^3} \int dE_{\nu_e} d\mu_{\nu_e} E_{\nu_e}^3 \mu_{\nu_e} f, \quad (4)$$

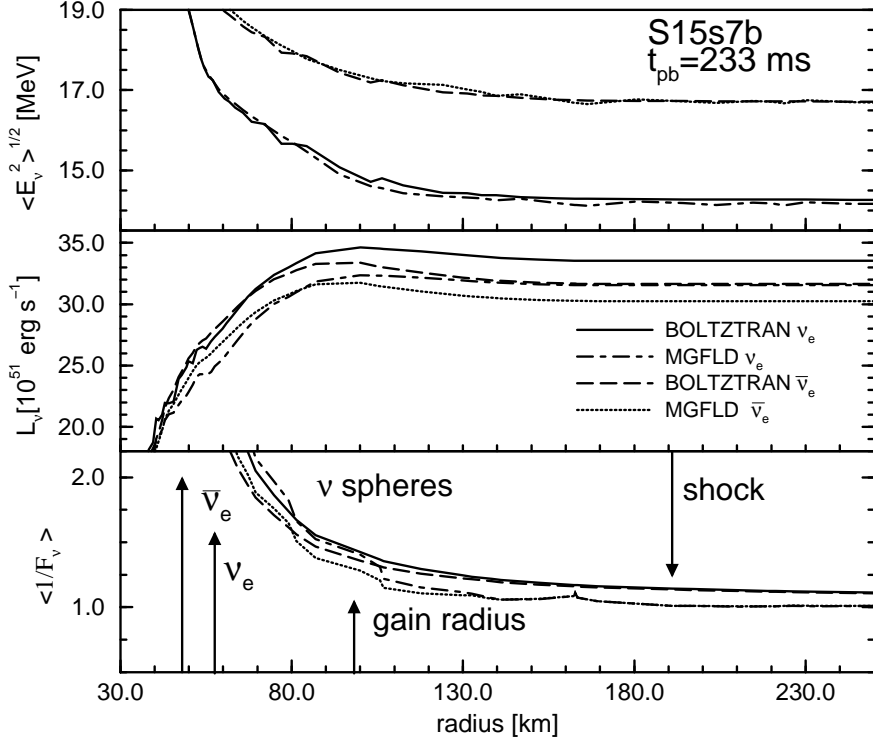


Figure 1. RMS energies, luminosities, and mean inverse flux factors for model S15s7b at 233 ms after core bounce.

$$\langle E_{\nu_e}^2 \rangle = \frac{\int dE_{\nu_e} d\mu_{\nu_e} E_{\nu_e}^5 f}{\int dE_{\nu_e} d\mu_{\nu_e} E_{\nu_e}^3 f}, \quad (5)$$

$$\langle \frac{1}{F} \rangle = \frac{\int dE_{\nu_e} d\mu_{\nu_e} E_{\nu_e}^3 f}{\int dE_{\nu_e} d\mu_{\nu_e} E_{\nu_e}^3 \mu_{\nu_e} f} = \frac{c U_{\nu_e}}{F_{\nu_e}}. \quad (6)$$

In equations (4)–(6),  $f$  is the electron neutrino distribution function, which is a function of the electron neutrino direction cosine,  $\mu_{\nu_e}$ , and energy,  $E_{\nu_e}$ . In equation (6),  $U_{\nu_e}$  and  $F_{\nu_e}$  are the electron neutrino energy density and flux. Corresponding quantities can be defined for the electron antineutrinos. Success or failure to generate explosions via neutrino reheating must ultimately rest on the three quantities defined in equations (4)–(6).

In Figure 1, at 233 ms after bounce for model S15s7b, we plot the electron neutrino and antineutrino RMS energies, luminosities, and mean inverse flux factors as a function of radius for our (8-point Gaussian quadrature) MGBT and MGFLD runs. The energy-averaged neutrinospheres (at 57 km and 48 km, for electron neutrinos and antineutrinos, respectively), and the location of the shock (at 191 km), are indicated by arrows. The gain radius (neutrino-energy integrated), located at 98 km, is also marked by an arrow. For the electron neutrinos, the differences in RMS energies between MGBT and MGFLD are at most 2% throughout most of the region plotted, although MGBT consistently gives higher energies. The differences between MGBT and MGFLD antineutrino RMS energies are smaller, and neither transport scheme yields consistently higher values. It should be noted that we expect larger differences when a fully hydrodynamic simulation is carried out, with MGBT giving harder spectra (Mezzacappa and Bruenn 1993a,c; see

also Burrows 1998). In a static matter configuration, differences that result from different treatments of the neutrino energy shift measured by comoving observers do not occur.

Significant differences between MGBT and MGFLD are evident when comparing the neutrino and antineutrino luminosities and mean inverse flux factors. Both transport methods compute similar electron neutrino luminosities until the neutrinospheres are approached from below. The antineutrino luminosities for each transport method also coincide up to this point. Just below the neutrinospheres, the MGBT luminosities diverge upward from the MGFLD luminosities, as MGFLD underestimates the neutrino flux, differing by 7% (4% for antineutrinos) at the neutrinospheres. After a decline from this maximum difference, the fractional difference grows from approximately 3% at the base of the gain region to a constant difference of 6% beyond about 170 km. Similar behavior is exhibited by the antineutrino luminosities, with the same fractional differences, 3% and 6%, obtained at the base of the gain region and near the shock, respectively.

For the electron neutrinos, the fractional difference between  $\langle 1/F \rangle_{\text{MGFLD}}$  and  $\langle 1/F \rangle_{\text{MGBT}}$  is 2%, 8%, and 12% at the neutrinosphere, gain radius, and shock, respectively. Just above the shock, the difference converges to 10% and is maintained to the edge of the core. Focusing on the semitransparent region,  $\langle 1/F \rangle_{\text{MGFLD}}$  is greater below the gain radius until the gain radius is approached; i.e., the MGFLD neutrino radiation field is more isotropic than the MGBT radiation field in this region. At 80 km, as the gain radius is approached, MGFLD computes a sharp decrease in  $\langle 1/F \rangle$ . This sharp decrease marks the radius at which the electron neutrino source is enclosed. The dip at 106 km and the sharp spike at 163 km in  $\langle 1/F \rangle_{\text{MGFLD}}$  are caused by local density perturbations.

For the electron antineutrinos, the same features are seen in  $\langle 1/F \rangle_{\text{MGFLD}}$ . The fractional difference is 0%, 11%, and 11% at the neutrinosphere, gain radius, and shock, respectively. The initial sharp decrease in  $\langle 1/F \rangle_{\text{MGFLD}}$  occurs at a smaller radius; the point at which the electron antineutrino source is enclosed is at a smaller radius. These results are typical of all three time slices.

Because each of the quantities plotted in Figure 1 is consistently greater for MGBT (while this is not strictly true for the antineutrino RMS energies in our stationary state comparisons, in a fully dynamical simulation these energies will be consistently higher for MGBT [Mezzacappa and Bruenn 1993a,c; see also Burrows 1998]), and because the neutrino heating rate is proportional to each of them, MGBT yields a significantly higher heating rate. As an example, just above the gain radius for model S15s7b, at  $t_{\text{pb}} = 233$  ms and the net-heating peak, MGBT yields a heating rate from neutrino absorption that is  $(102\%)^2 \times 110\% \times 112\%$  of the MGFLD rate.

In Figure 2, for MGBT and MGFLD, we plot the *net* neutrino heating rates as a function of radius for model S15s7b at  $t_{\text{pb}} = 233$  ms. (As discussed in Section 2, the results from four Gaussian quadrature sets are plotted to demonstrate numerical convergence.) These rates include the contributions from both the electron neutrinos and antineutrinos, and were computed using the following formulae:

$$(d\epsilon/dt)_i = c \int E_\nu^3 dE_\nu [\psi_i^0 / \lambda_i^{(a)} - j_i(1 - \psi_i^0)] / \rho(hc)^3 \quad (7)$$

where  $\epsilon$  is the internal energy per gram;  $E_\nu$ ,  $\psi_i^0$ ,  $\lambda_i^{(a)}$ , and  $j_i$  are the electron neutrino or antineutrino energy, zeroth angular moment, absorption mean free path, and emissivity,

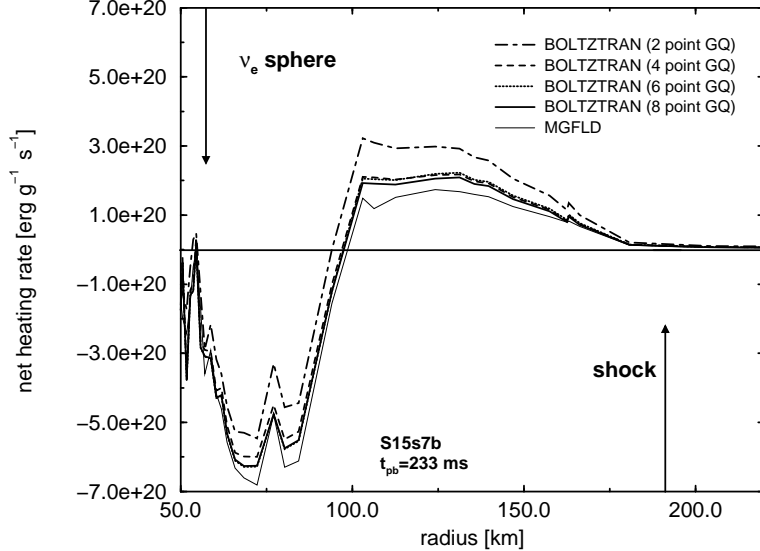


Figure 2. Net heating rates for model S15s7b at 233 ms after core bounce.

respectively;  $i = 1$  corresponds to electron neutrinos, and  $i = 2$  corresponds to electron antineutrinos. Only the contributions from neutrino emission and absorption were included. The MGBT simulation yields a net heating rate just above the gain radius that is  $\sim 1.3$  times the MGFLD rate, and a net cooling rate below the gain radius that is consistently  $\sim 0.8$  times the MGFLD rate. The differences in net heating rate are even greater for the  $t_{\text{pb}} = 106$  ms time slice in our  $15 M_{\odot}$  model and for the  $t_{\text{pb}} = 156$  ms time slice in our  $25 M_{\odot}$  model (cf. Table 1 and Messer *et al* 1998).

#### 4. Summary, Discussion, and Conclusions

Comparing three-flavor MGBT and three-flavor MGFLD in postbounce supernova environments, we find that MGBT leads to a significant increase/decrease in the *net* heating/cooling rate, particularly just above/below the gain radius. The MGBT net heating rate can be as much as 2 times the MGFLD net heating rate above the gain radius, with net cooling rates that are typically 0.8 times the MGFLD rate below. These differences stem primarily from differences in the neutrino luminosities and mean inverse flux factors; the heating rate is linearly proportional to both these quantities, and differences in both add to produce a significant difference in the net heating rate.

We also observe that the differences in the net heating rate are greatest at earlier postbounce times for a given progenitor mass, and at a given postbounce time, greater for greater progenitor mass. This is illustrated in Table 1. The enhancement in heating with increased progenitor mass suggests that the net heating enhancement from MGBT is potentially robust and self-regulated.

In closing, our results are promising, and their ramifications for core collapse supernovae, and in particular, for the postbounce neutrino-heating, shock-revival mechanism, await one- and two-dimensional dynamical simulations with MGBT coupled to the core hydrodynamics. One-dimensional simulations are currently underway, and we plan to report on them soon.

Table 1. Maximum Net Heating/Cooling Rates

Progenitor Mass [ $M_{\odot}$ ]	$t_{pb}$ [ms]	Maximum Net Heating Ratio	Maximum Net Cooling Ratio
15	106	2.0	0.8
	233	1.3	0.8
25	156	2.0	0.8

## 5. Acknowledgements

BM was supported at the University of Tennessee under NASA grant NRA-96-04-GSFC-073. AM and MWG were supported at the Oak Ridge National Laboratory, which is managed by Lockheed Martin Energy Research Corporation under DOE contract DE-AC05-96OR22464, and at the University of Tennessee, under DOE contract DE-FG05-93ER40770. SWB was supported at Florida Atlantic University under NASA grant NRA-96-04-GSFC-073 and NSF grant AST-9618423. The simulations presented in this paper were carried out on the Cray C90 at the National Energy Research Supercomputer Center, the Cray Y/MP at the North Carolina Supercomputer Center, and the Cray Y/MP and Silicon Graphics Power Challenge at the Florida Supercomputer Center. AM and SWB gratefully acknowledge the hospitality of the Institute for Theoretical Physics, Santa Barbara, which is supported in part by the National Science Foundation under grant number PHY94-07194.

## References

Bethe H & Wilson J R 1985 *ApJ* **295** 14  
 Bowers R L & Wilson J R 1982 *ApJS* **50** 115  
 Bruenn S W 1985 *ApJS* **58** 771  
 Bruenn S W 1993 *Nuclear Physics in the Universe* (Bristol: IOP Publishing) p 31  
 Burrows A 1998 *Proceedings of the 18th Texas Symposium on Relativistic Astrophysics* (Singapore: World Scientific Press) in press  
 Burrows A & Goshy J 1993 *ApJ* **416** L75  
 Janka H-Th, & Müller, E. 1996 *A&A* **306** 167  
 Lattimer J M & Swesty F D 1991 *Nucl. Phys. A* **535** 331  
 Levermore C D & Pomraning G C 1981 *ApJ* **248** 321  
 Messer O E B, Mezzacappa A, Bruenn S W, & Guidry M W 1998 *ApJ* submitted  
 Mezzacappa A & Bruenn S W 1993a *ApJ* **405** 637  
 ——— 1993b *ApJ* **405** 669  
 ——— 1993c *ApJ* **410** 710  
 Mezzacappa A, Calder A C, Bruenn S W, Blondin J M, Guidry M W, Strayer M R, & Umar A S *ApJ* **495** 911  
 Mezzacappa A & Matzner R A 1989 *ApJ* **343** 853  
 Myra E, Bludman S, Hoffman Y, Lichtenstadt I, Sack N & Van Riper K 1987 *ApJ* **318** 744  
 Swesty F D & Lattimer J M 1994 *ApJ* **425** 195  
 Wilson J R 1985 *Numerical Astrophysics* (Boston: Jones & Bartlett) p 422  
 Wilson J R & Mayle R W 1993 *Phys. Rep.* **227** 97  
 Woosley S E 1995 private communication